Digital Twin-Enabled Response Function Analysis: A Synthetic Approach to Ship's Propulsion System Assessment

Oleksiy Bondarenko[1,*] and Yasushi Kitagawa[2]

ABSTRACT

Analyzing the behavior of vessels in actual sea conditions is crucial for conceptual system design, safety and energy efficiency considerations. However, the essential seakeeping problem is reduced to the analysis of wave-hull interactions often neglecting consideration of the propulsion. But in the meantime, the synthetic consideration of wave–propulsion interactions is a key for safety and energy efficiency. Furthermore, safety evaluation of a ship's design with reduced propulsion power in adverse seas is vital for risk management. Response functions are commonly used to estimate propulsion system responses in incoming seaways. This paper proposes a synthetic approach using digital twin technology for rapid response function estimation. It introduces a companion linearized state-space model linked with the digital twin, enabling immediate retrieval of coefficients for response function analysis at the desired operating point. This integrated methodology provides a comprehensive representation of ship propulsion behavior in wave environments, offering a comprehensive framework for system performance assessment.

KEY WORDS

Propulsion system; state-space model; propulsion system dynamics; describing function analysis.

INTRODUCTION

Over the last decade, concerns about environmental issues have spurred the maritime industry to undergo a major shift towards zero-emission shipping. Digital transformation is considered one of the drivers in transforming the maritime industry into a more sustainable and efficient transportation sector. With the advent of the Internet of Things (IoT) and the development of sensors and monitoring systems, a wide variety of data has become available for processing onboard or at on-shore data centres, delivering a number of new possibilities. However, raw data is of little value until it is turned into information to enable knowledge. In this context, the advancement in the digitalization of ship operations and the imperative to turn the raw data into knowledge for informed decision-making, have given rise to the development of another emerging technology – a digital twin. The digital-twin is an accurate virtual replica of its physical counterpart, that delivers valuable information by mapping the dynamic behavior in real time. For example, simulation-based analysis of operational data, where the error between predicted and actual responses may uncover system abnormalities. However, the utilization of such a complex tool cannot be justified as a universal tool for all kinds of applications. In particular, when it comes to predicting the expected significant value of a response ahead of time for a known spectrum of input disturbance, the response functions (derived from linear models) are preferable. Furthermore, the ship's hull seakeeping performance is commonly evaluated by using the response functions which translate waves into hull motion responses for a given wave frequency. In turn, wave and hull motions are the main cause of propeller torque fluctuation that disturbs the operation of the propulsion engine. Thus, the synthetic representation of the hull-propeller-engine mutual responses is highly relevant for the safety assessment of the ship propulsion system operation, especially in operation under extreme propeller load torque fluctuations (Sui 2022).

---

[1] Marine Environment and Engine System, National Maritime Research Institute, Tokyo, Japan;

[2] Fluid Engineering and Ship Performance Evaluation, National Maritime Research Institute, Tokyo, Japan;

* Corresponding Author: bond@m.mpat.go.jp

An early attempt at a synthetic consideration of ship propulsive performance in waves dates back to the late 70s (Naito 1979), where the linearized representation of the mutual relations among the functions of a ship propulsion system was derived and used for the prediction of speed loss of the ship in waves. Later Kim (1985) expanded the consideration of the ship propulsion system for the evaluation of propulsive dynamics in rough sea conditions. Recently, a notable effort on propulsion system dynamics and behavior in the time and frequency domains was made by Xiros (2002), where a linearized model is used for engine speed control synthesis, also taking into account turbocharger-engine interaction. An analysis of complex and extreme propeller-engine interaction in the case of ventilation and racing is reported by Bondarenko (2011, 2012). A more recent development of a linear representation of the core propulsion system is reported by Stapersma (2017) and in a companion paper by Vrijdag (2017). In that research, the linearized model of both uncontrolled and controlled systems was derived and used for time and frequency domain analysis of propulsion plant behavior in waves. It was concluded that the linearized model is a suitable tool for system analysis and controller development as long as the limitations of linearization are kept in mind.

Although a variety of linearization procedures and response function models can be found in the literature, an accurate estimation of the propulsion system response function requires detailed information about characteristics intrinsic to propulsion components such as hull, propeller, and engine; in the early stages of ship design, might not be available. Furthermore, ship in-service is characterized by a significant degree of uncertainty, and for this reason, the response function estimated from the "ideal" theoretical characteristics may not fit the actual system. At the same time, the digital twin binds information/data sources of the physical space, a set of dynamic models describing the physical counterpart, and a set of parametrized characteristics, parameters of which are instantiated explicitly for the specific ship in service. Thus, owing to the explicit functional relationships and parametrized characteristics at the core of the digital twin, the linearized representation of the propulsion system can be derived analytically.

This paper intends to provide a synthetic approach binding the identified parametrized models of the digital twin and the companion linearized state-space model, where the data feedback from the ship in service can be used to assess the propulsive performance in waves and review future ship designs. Moreover, to account for the engine torque limit function, the linearized model of the propulsion system was extended with a describing function - a quasi-linear representation of the hard nonlinearity.

THE BASE SHIP PROPULSION SYSTEM

In the context of the defined objective, which is the assessment of the propulsive performance of a ship in waves, a generic ship propulsion system may be considered to be made of three main components: an engine producing the torque, a shaft transmitting the torque from the engine to the propeller, and a propeller delivering thrust to a hull. Additionally, the engine speed governor, which is a part of the engine, forms the shaft speed control loop. Figure 1 details the composition and mutual relations among the functions of the components.

The ship's hull translation (surge) motion is based on a force balance between propeller thrust and hull resistance:

$$(m + m_x)\frac{dV_s}{dt} = T_p - R_t, \quad R_t = R_c + X_w \quad [1]$$

where m and m_x are the constant hull mass and added mass, correspondingly; T_p is the effective propeller thrust, R_t is the total water resistance composed of calm water component, R_c, and the added resistance due to waves, X_w. Here, it is worth noting that only time-averaged steady waves-induced forces acting on the ship hull are considered. In contrast, the time-varying oscillatory forces are neglected since the time scale is much shorter than that of the hull longitudinal velocity, Vs. Thus, equation [1] determines the steady-state position of the engine operating point.

The propulsion engine is directly interfaced with the propeller by means of shaft rotational dynamics, expressed as:

$$2\pi I_{sh}\frac{dn_{sh}}{dt} = Q_e - Q_p \quad [2]$$

where Q_e, Q_p are the engine and propeller torques, respectively, I_{sh} is the moment of inertia of the rotating shaft system, including the engine, propeller and added mass of water, n_{sh} is the propeller shaft rotational speed which is also equivalent to the engine rotational speed, in case of direct coupling of propeller and engine. Note that the shaft speed control loop is also a part of the propulsion system, and the details will be covered later.
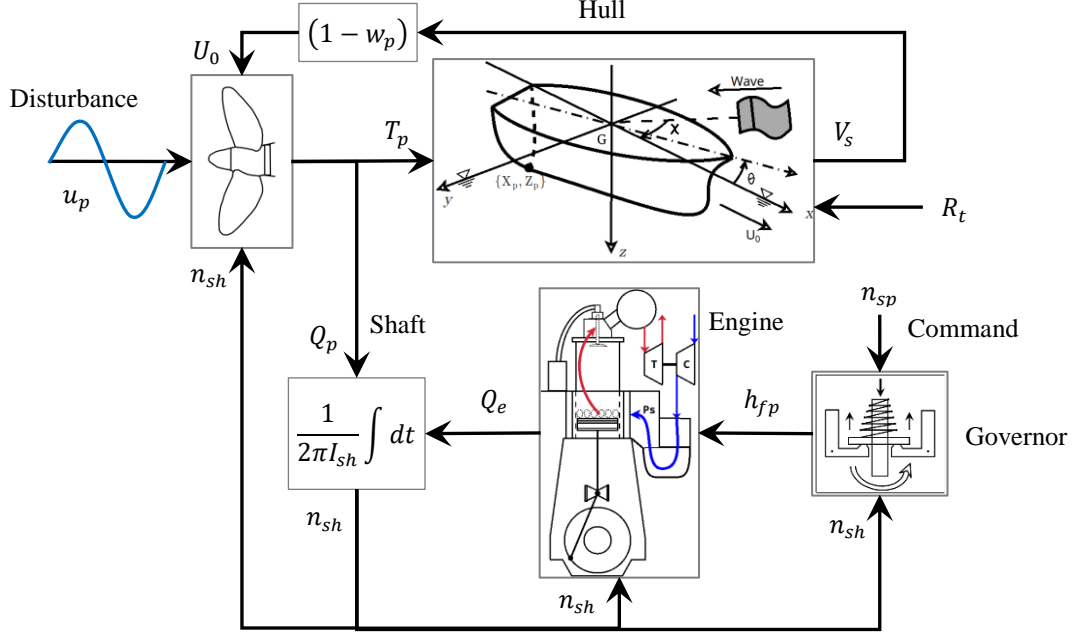
Figure 1: The base ship propulsion system

The static models of the effective propeller thrust and torque are based on the propeller open-water characteristics obtained in calm water conditions. These are given as follows:

$$T_p = \left(1 - t_p\right)\rho n_{sh}^2 D_p^4 K_t\left(J\right)$$

$$Q_p = \rho n_{sh}^2 D_p^5 K_q\left(J\right)\frac{1}{\eta_r}$$

$$J = \frac{U_p}{n_{sh}D_p}, \quad \because U_p = U_0 + u_p\left(t\right), \quad U_0 = V_s\left(1 - w_p\right)$$

[3]

where t_p is the thrust deduction ratio, w_p is the wake fraction, ρ is the water density, D_p is the propeller diameter, J is the propeller advance ratio, K_q, K_t are the torque and thrust coefficients expressed as polynomial functions of the J, defined by an open propeller characteristic, η_r is the propeller relative rotation efficiency, and U_p is the effective inflow velocity composed of the steady-part, U_0, and fluctuating part, $u_p(t)$. The time-varying forces induced by waves on the ship's hull excite oscillatory hull motions, which, in turn, along with the wave orbital motion, induce a time-varying velocity field around the propeller. The in-line or axial component, $u_p(t)$, of the velocity field, gives rise to a change in the advance velocity U_p and consequently the advance ratio J. With time-varying J, the propeller operating point is moving on the K_q curve, inducing fluctuation in the propeller torque and, consequently, engine torque and revolution. Thus, effective inflow velocity acts as a link between wave-hull interaction and propeller-engine response, provided that the base ship propulsion system can be split into separate parts, and each can be investigated independently. Figure 2 illustrates the boundaries of each part.
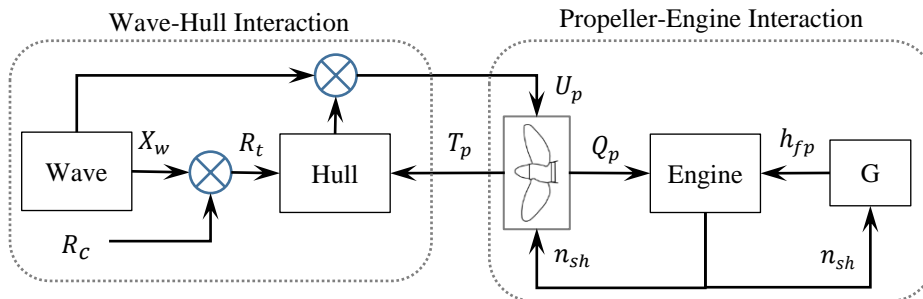

Figure 2: Decomposition of base ship propulsion system

Engine Model

Internal combustion engines remain an unavoidable part of the ship propulsion system, owing to the efficient conversion of fuel chemical energy into mechanical energy. The vast majority of merchant ships use low-speed, two-stroke marine Diesel engines as a prime mover. The objective of the engine model is to represent an external characteristic of the engine concerning the developed torque, which in the general case is a function of engine states such as rotational speed and air and fuel mass flows (Xiros 2002). In the field of propulsion system simulation, a cycle-mean value (CMV) engine modelling approach is commonly used for steady-state and transient performance evaluation (Hendrics 1989, Theotokatos 2010). The central assumption in the CMV modeling approach is that air and exhaust gases flow continuously irrespective of the intermittent nature of a cylinder scavenging process. Thus, the engine is considered a series of control volumes connected through flow restrictions, ensuring continuity of air and exhaust gas flows. The engine is decomposed into a finite number of elements, including the cylinder, air and exhaust gas receivers, turbocharger (TC) with a compressor and turbine, and an air cooler, as shown in figure 3 below.
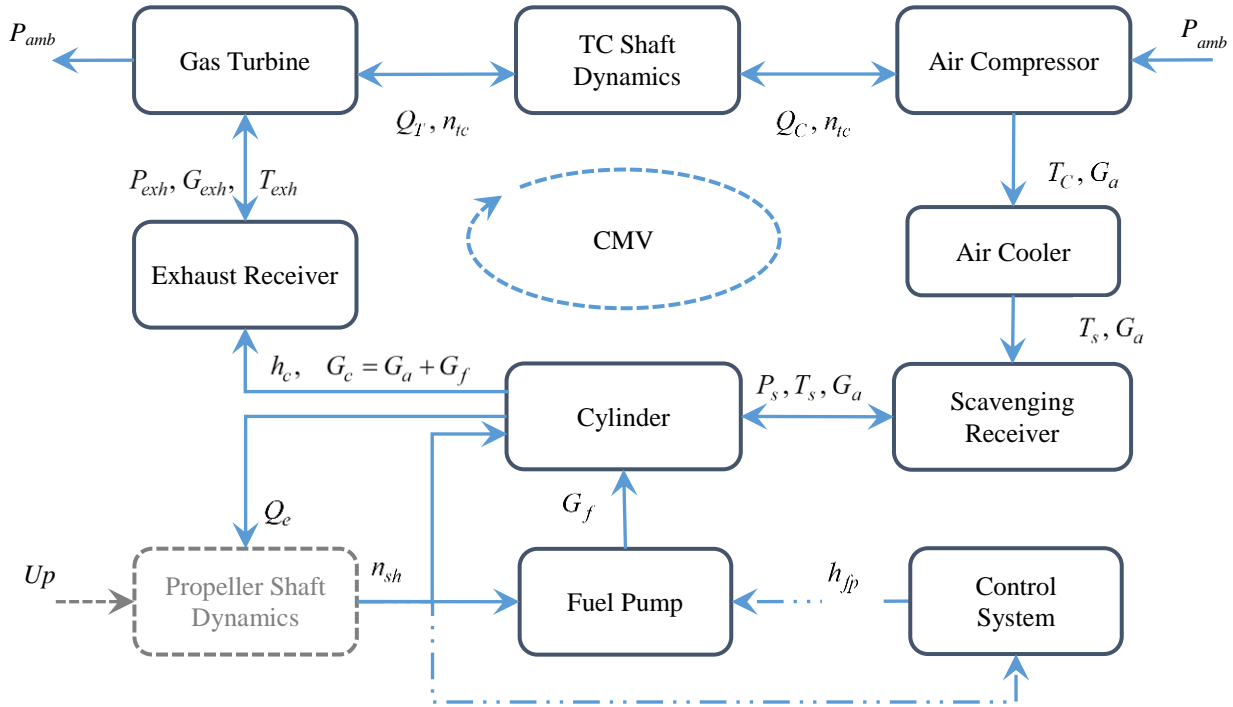

Figure 3: Composition of the propulsion engine

The compressor and turbine are mechanically linked via the TC shaft. An air cooler is connected between the compressor and the air receiver. The fuel pump, i.e. fuel injector, is directly connected to the cylinder. The engine's cylinders are linked with the propeller through shaft rotational dynamics, expressed by the equation [2]. In turn, the engine torque is the result of an indicated mean effective pressure (IMEP), P_i, developed in the cylinder volume V_s during one cycle, minus a friction mean effective pressure (FMEP), P_f:

$$Q_e = \frac{\left(P_i - P_f\right)V_s}{2\pi}$$

[4]

The developed IMEP is a function of the engine states such as pressures, p, temperatures, T, and mass flows, G. The fundamental equations necessary to describe the temporal evolution of the engine state variables can be obtained from the following mass and energy conservation laws along with the ideal gas equation:

$$\frac{dm}{dt} = \sum_i G_i, \quad i \in \{a, exh, f\}$$

[5]

$$p = \frac{m}{V}\tilde{R}T \quad \Rightarrow \quad \frac{dp}{dt} = \frac{dm}{dt}\frac{\tilde{R}T}{V} = \frac{\tilde{R}T}{V}\left(\sum_i G_i\right), \quad \because T = \text{const} \qquad [6]$$

$$c_v m \frac{dT}{dt} + u \frac{dm}{dt} = \sum_i h_i G_i \qquad [7]$$

here u is the internal energy, $\check{R}$, c_v are the thermodynamic constants, and m is the mass of the gas.
The air and exhaust gas mass flow rates, through the engine and turbine, respectively, are calculated under the assumption that an orifice with the equivalent mean effective flow area $\mu\check{A}$ can characterize the engine cylinder as well as turbine. Thus, the flow of compressible gas is evaluated according to:

$$G_{(a,exh)} = \mu\tilde{A} \frac{p_{in}}{\sqrt{RT_{in}}} \Psi\left(p_{in}, p_{out}\right) \qquad [8]$$

here, the subscripts, in/out, represent the inlet and outlet parameters of the considered element, correspondingly. $\Psi = f(p_{in}, p_{out})$ is the throttling characteristic of the orifice.

The turbocharger, which is an integral part of the engine, contributes to the assurance of sustainable airflow necessary for optimal and efficient fuel combustion. The dynamic of the turbocharger, in terms of the rotational speed, is derived by applying the angular momentum conservation in the following form:

$$2\pi I_{tc} \frac{dn_{tc}}{dt} = Q_T - Q_C \qquad [9]$$

$$Q_T = \frac{\eta_{iT}}{2\pi n_{tc}} G_{exh} C_{p.e} T_{exh} \left[1 - \left(\frac{P_{amb}}{P_{exh}}\right)^{\frac{k_e-1}{k_e}}\right] \qquad [10]$$

$$Q_C = \frac{G_a C_{p.a} T_{amb}}{2\pi n_{tc} \eta_{iC}} \left[\left(\frac{P_s}{P_{amb}}\right)^{\frac{k_a-1}{k_a}} - 1\right] \qquad [11]$$

where Q_T is the torque developed by the turbine due to the expansion of exhaust gas from pressure P_{exh}, Q_C is the torque required by the compressor to compress the air to pressure P_s in the scavenging receiver, n_{tc} is the turbocharger rotational speed, I_{tc} is the inertia of the turbocharger shaft, η_{iC}, η_{iT} are the isentropic efficiencies of the compressor and turbine, correspondingly.

The energy flow rate, $h_c G_c$, exiting the engine cylinder and taking part in the energy balance of the exhaust gas receiver in equation [7], is calculated by taking into consideration the energy conservation in the cylinder, averaged over one engine cycle, thus:

$$h_c G_c = G_a C_{p.a} T_s + G_f H_U - W_i, \quad \because W_i = \oint p_c dV \qquad [12]$$

where W_i is the engine cylinder indicated work, which is the result of one complete engine cycle calculation. In the CMV approach, however, the complete combustion cycle simulation, as commonly accepted (Xiros 2002, Theotokatos 2010), has been seamlessly embedded by the coefficient ζ_a, which denotes the proportion of the fuel chemical energy retained in the exhaust gas:

$$\zeta_a = 1 - \frac{W_i}{G_f H_U} \qquad [13]$$

Thus, the energy rate of exhaust gas is considered an increase in the energy rate of scavenging air due to combustion in the following form:

$$h_c G_c = G_a C_{p.a} T_s + \zeta_a G_f H_U \qquad [14]$$

This, admittedly, fosters the successful transition to the transfer function representation.

The engine fuel mass flow rate, G_f, is calculated as a linear function of the fuel pump index, F_p, as follows:

$$G_f = Z_c m_{fc_{mcr}} h_{fp} n_{sh} \qquad [15]$$

where m_{fc_mcr} is the mass of fuel injected per cycle at MCR, Z_c is the number of engine cylinders, and h_{fp} is the fuel pump index determined by the engine control system. The subscript 'mcr' denotes values at the MCR point of the engine.

Finally, in the quasi-steady context of CMV, the IMEP is considered proportional to the fuel pump index, as follows:

$$P_i = \eta_{C_{eff}} P_{i_{mcr}} h_{fp} \qquad [16]$$

Indeed, increasing the fuel index leads to an increase in the fuel amount per cycle per cylinder and thus a higher IMEP, provided that a perfect combustion regime is maintained. The latter holds true for the most practical operating points along propeller lines. However, in actual sea conditions, when the engine operating point most likely shifts towards a region of low speed and high torque the ability of the compressor to supply air for combustion tends to decrease. Consequently, the combustion process becomes more susceptible to variations in air-to-fuel ratio (AFR). Moreover, in transient conditions, the fuel amount, determined by the fuel index, h_{fp}, adjusts sufficiently fast following the demand in engine torque to keep the engine speed constant, as shown by equation [2]. At the same time, the air mass flow may be delayed compared to that of fuel due to the large inertia of the TC and the lack of a mechanical connection between the TC and the engine shaft. Indeed, the energy of the exhaust gas delivered to the turbine must first accelerate the TC shaft for the compressor to develop air pressure before the cylinder, imposing additional delay due to the presence of the exhaust gas and air receivers in between. Thus, in transient conditions, due to the engine response to propeller load fluctuation, the optimal AFR ceases to hold due to the delay in air supply, leading to engine performance degradation. Such a phenomenon clearly must be accounted for in the dynamic engine model. Therefore, the IMEP in equation [16] is modified with the coefficient η_{Ceff}, introduced (Medica 1988, Xiros 2002) to take into account the losses due to incomplete fuel combustion. Furthermore, a series of theoretical and experimental studies (Bondarenko, 2018; Bondarenko, 2023) have revealed the characteristics of combustion process degradation due to the depletion of air charge in the cylinder. Thus, the following combustion efficiency coefficient is introduced into the model:

$$\eta_{C_{eff}} = f\left(AFR\right) = C_0 AFR^{\frac{b_0}{AFR}}, \quad \therefore AFR = \frac{G_a}{G_f} \qquad [17]$$

where C_0 and b_0 are the coefficients that represent the sensitivity of combustion efficiency to the AFR. Figure 4 illustrates a family of characteristics for different coefficient selections. As can be observed, the adopted model demonstrates a consistent decline in combustion efficiency when AFR falls below the nominal value (AFR < 1.0), grounded on the experimental results.
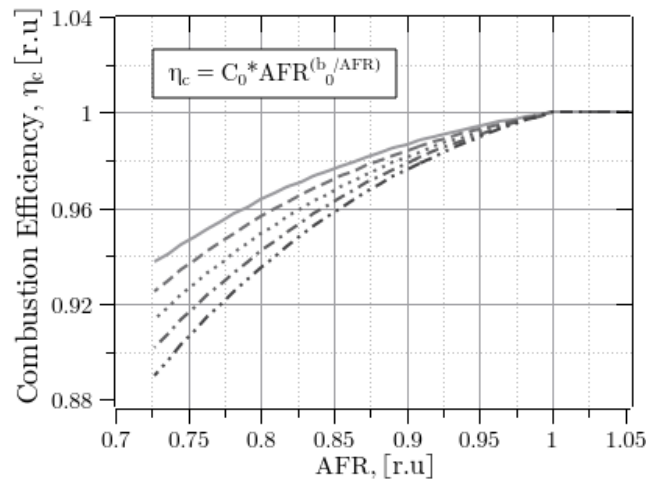

Figure 4: Combustion efficiency characteristics

Apart from the presented fundamental algebraic and differential equations describing the engine components' behavior, there are certain empirical characteristics required to complete the model. These include effective turbine area, $\mu\tilde{A}$, compressor isentropic efficiency, η_{iT}, remained fuel energy proportion in exhaust gas, ζ_a, FMEP, P_f, defined as follows:

$$\mu \tilde{A} = c_{\mu_0} + c_{\mu_1} \left(\frac{P_{amb}}{P_{exh}} \right) + c_{\mu_2} \left(\frac{P_{amb}}{P_{exh}} \right)^2 \tag{18}$$

$$\eta_{iT} = \eta_{iT_0} \left[\frac{n_{tc}}{C_s} \left(c_{T_0} - \frac{n_{tc}}{C_s} \right) + c_{T_1} \right] \tag{19}$$

$$\zeta_a = c_{\zeta_0} + c_{\zeta_1} \frac{Q_e}{Q_{e_{mcr}}} \tag{20}$$

$$P_f = P_{i_{mcr}} \left(c_{f_0} + c_{\zeta_1} \frac{n_{sh}}{n_{sh_{mcr}}} + c_{\zeta_2} h_{fp} \right) \tag{21}$$

The outlined CMV modelling approach results in continuous, nonlinear, and fully parameterized first-order ordinary differential equations, describing the time evolution of the key engine states, as shown below. Such model formulation allows for the analytical transition to the linear state-space model, ensuring the effective binding of the linear counterpart to the original nonlinear model.

$$\frac{d}{dt} \boldsymbol{Y}(t) = \boldsymbol{F}\left(\boldsymbol{Y}, \boldsymbol{\theta}, h_{fp}, u_p \right), \quad \boldsymbol{Y} = \left[n_{sh}, n_{tc}, P_s, M_{exh}, T_{exh} \right]^T \tag{22}$$

here $\boldsymbol{Y}$ is the vector of state variables, $\boldsymbol{\theta}$ is a set of constants that parametrize the static characteristics of the engine components, h_{fp} is the input from a control system, and u_p is the disturbance resulting from the wave-hull interaction.

In past research (Bondarenko 2020, Bondarenko 2023) the adaptive parameters identification framework was developed. The framework integrates the core of the digital twin - a set of parametrized dynamic models - with information/data sources of the physical space. It is possible to identify the constants that parametrize the static characteristics of the engine components, tailored to the specific ship in service, in this way.

Engine Control System

The control system of marine diesel engines aims at controlling their speed and load operating regimes. Inadequate control system dynamics may lead to incomplete fuel combustion, thermal and mechanical overload of the engine components, and excessive oscillation of the shaft rotational speed. As a rule, the control system of propulsion engines consists of a speed governor and several functional modules for protection against torque and thermal overloading. For the purpose of the present study, a Proportional-Integral (PI) + Proportional (P) governor structure is used as shown in figure 5 in the form of the Laplace domain block diagram (Gorb 1989). The PI+P structure mimics a popular and classic hydro-mechanical governor of Woodward. The linear part of the governor's dynamic can be represented in state-space form, as demonstrated below:

$$\frac{d}{dt} \boldsymbol{x} = \boldsymbol{A} \boldsymbol{x} + \boldsymbol{B} u, \quad \boldsymbol{x} = \left[\bar{X}_{efb}, \bar{X}_{pp} \right]^T, \quad u = \left[\left(n_{sp} - n_{sh} \right) \right]$$

$$y = \boldsymbol{C} \boldsymbol{x}, \qquad y = h_{fp}$$

$$\boldsymbol{A} = \begin{bmatrix} -\left(\frac{K_i K_m K_{su}}{T_{ss}} + \frac{1}{T_i} \right) & -\frac{K_i K_m K_{fb} K_{su}^2}{T_{ss}} \\ -\frac{K_m}{T_{ss}} & -\frac{K_{fb} K_m K_{su}}{T_{ss}} \end{bmatrix}, \boldsymbol{B} = \begin{bmatrix} -\frac{K_i K_m K_{su}}{T_{ss}} \\ -\frac{K_m}{T_{ss}} \end{bmatrix}, \boldsymbol{C} = \begin{bmatrix} 0 & 1 \end{bmatrix} \tag{23}$$
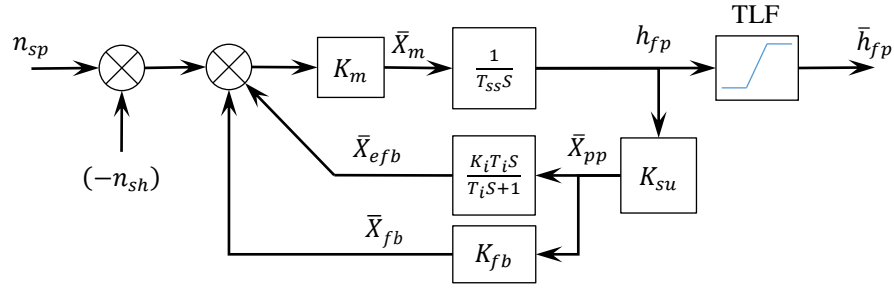
Figure 5: Governor functional block diagram

In order to prevent the engine from thermal and mechanical overloads, the engine control system includes a torque limiter function (TLF). The TLF provides saturation of the governor output at the upper boundary, limiting the fuel injection amount, and thus engine torque. Figure 6 illustrates characteristics of TLF implemented in the governor.
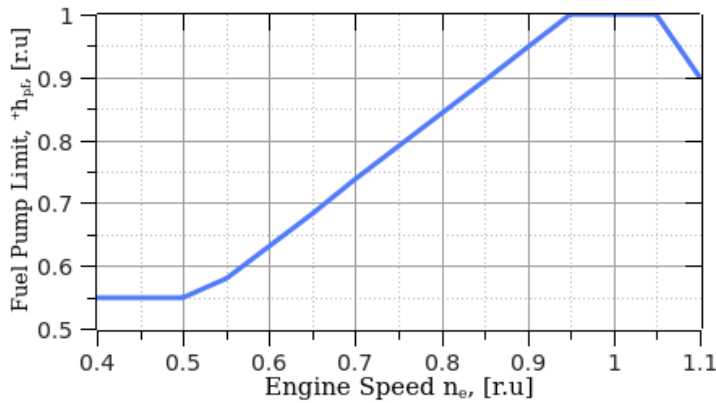

$$h_{fp} = \begin{cases} h_{fp}, \text{if } h_{fp} \le {}^+h_{fp} \\ {}^+h_{fp}, \text{if } h_{fp} > {}^+h_{fp} \end{cases}$$

$$^+h_{fp} = \begin{cases} 0.55, \text{if } n_e \le 0.5 \\ \dfrac{n_e}{0.95}, \text{if } 0.5 < n_e \le 0.95 \\ 1.0, \text{if } n_e > 0.95 \end{cases} \qquad [24]$$

Figure 6: The TLF characteristic

THE STATE-SPACE MODEL OF THE PROPELLER-ENGINE SYSTEM

As noted earlier, wave and hull motions are the main causes of propeller torque fluctuation, disturbing the operation of the propulsion engine. The response functions conveniently relate the system's response to a forcing function with the aid of appropriate Laplace transforms. Thus, the response functions, which translate waves into hull motions and, in turn, into propeller torque fluctuation, characterize the wave-hull-propeller interaction in the frequency domain (Bondarenko 2011). It is desirable to interface these characteristics into the analysis of propeller-engine interaction, resulting in a comprehensive assessment of hull-propeller-engine interaction. Since the equations representing propeller-engine interaction are non-linear differential equations, the linearization about an operating point is required. The response functions are obtained from the linear state-space representation for input disturbance.

Different types of nonlinearities intrinsic to the system require different linearization techniques. Thus, for weak types, such as nonlinearity due to the product of variables or nonlinearity due to polynomial characteristics, the standard approach, often called small signal increments, is the most suited. Whereas hard nonlinearity, such as saturation, requires a special technique often called harmonic linearization. At first, the linearization of the base propulsion system without TLF will be presented, followed by the introduction of describing function for a (quasi) linear description of the TLF.

Linearization

The basic method of small increments is commonly used for the linearization of propulsion engine models (Mezherickiy 1971, Naito 1979, Stapersma 2017). The method allows for interpreting a nonlinear function as an explicit linear combination of the small increments of the constituent variables, simultaneously getting rid of constant parameters. For the sake of simplicity and illustration of the application of the method, the nonlinear equation of propeller shaft dynamics, equation [2],

will be processed from now on. Let's rewrite the equation [2] in the form of finite increments of the constituent variables about a steady-state operating point, simultaneously introducing normalization at that point:

$$\frac{2\pi I_{sh}}{Q_{P_0}}\frac{d\Delta n_{sh}}{dt}\frac{n_{sh_0}}{n_{sh_0}} = \frac{\Delta Q_e}{Q_{P_0}} - \frac{\Delta Q_p}{Q_{P_0}}, \quad Q_{e_0} \equiv Q_{P_0}, \quad \frac{\Delta n_{sh}}{n_{sh_0}} \equiv \delta n_{sh}, \quad \frac{\Delta Q_e}{Q_{P_0}} \equiv \delta Q_e, \quad \frac{\Delta Q_p}{Q_{P_0}} \equiv \delta Q_p$$

$$\Downarrow$$

$$\frac{d}{dt}\delta n_{sh} = \frac{1}{\tau}\left[\delta Q_e - \delta Q_p\right], \quad \tau = \frac{2\pi I_{sh}}{Q_{P_0}}n_{sh_0}$$

[25]

Equation [25] requires further detailing of the torque functions, and following the method of small increments, the composite functions are decomposed by applying a logarithm, and then the partial differentiation is performed. Finally, by introducing coefficients of influence and substituting finite increments for differentials, the composite function is replaced by a linear combination of constituent variables. Thus, the transformation of the propeller torque function defined in equation [3] yields:

$$Q_p = \rho n_{sh}^2 D_p^5 K_q(J)\frac{1}{\eta_r}$$

$$\Downarrow$$

$$\ln(Q_p) = \ln(\rho) + 2\ln(n_{sh}) + 5\ln(D_p) + \ln(K_q) - \ln(\eta_r)$$

$$\Downarrow$$

$$\frac{dQ_p}{Q_{P_0}} = 2\frac{dn_{sh}}{n_{sh_0}} + \frac{dK_q}{K_{q_0}}, \quad \frac{dQ_p}{Q_{P_0}} \approx \frac{\Delta Q_p}{Q_{P_0}} \equiv \delta Q_p, \dots$$

$$\Downarrow$$

$$\delta Q_p = 2\,\delta n_{sh} + \delta K_q$$

[26]

The torque coefficient, K_q, holds the nonlinear functional relation in the polynomial form with the engine speed and inflow velocity and thus requires further linearization. Applying the Taylor series expansion, neglecting higher order term, the transformation yields:

$$K_q(J) = q_o + q_1 J + q_2 J^2, \quad J = \frac{U_p}{n_{sh}D_p}$$

$$\Downarrow$$

$$\Delta K_q = \frac{\partial K_q}{\partial n_{sh}}\Delta n_{sh} + \frac{\partial K_q}{\partial U_p}\Delta U_p$$

$$\Downarrow$$

$$\frac{\Delta K_q}{K_{q_0}} = \underbrace{\frac{\partial K_q}{\partial n_{sh}}\frac{n_{sh_0}}{K_{q_0}}}_{k_{q_1}}\frac{\Delta n_{sh}}{n_{sh_0}} + \underbrace{\frac{\partial K_q}{\partial U_p}\frac{U_{P_0}}{K_{q_0}}}_{k_{q_2}}\frac{\Delta U_p}{U_{P_0}}, \quad \frac{\Delta K_q}{K_{q_0}} \equiv \delta K_q, \dots$$

$$\Downarrow$$

$$\delta K_q = k_{q_1}\delta n_{sh} + k_{q_2}\delta u_p$$

[27]

Substituting the result of equation [27] into the result of equation [26] and collecting coefficients for the same variables, the transformation yields the following result:

$$\delta Q_p = \left(2 + k_{q_1}\right)\delta n_{sh} + k_{q_2}\delta u_p$$

[28]

Under similar considerations, the finite increment of engine torque, δQ_e, can be derived in the following form:

$$\delta Q_e = k_{imep} k_{C_{eff}} \left(\delta G_a - \delta G_f \right) + k_{imep} \delta h_{fp} - k_{fmep} \delta n_{sh}$$

$$\delta G_a = \left(1 - k_{\Psi_a} \right) \delta P_s + k_{\Psi_a} \left(\delta M_{exh} + \delta T_{exh} \right) \qquad [29]$$

$$\delta G_f = \delta h_{fp} + \delta n_{sh}$$

The unwieldy expression for the engine torque results from the presence of the combustion efficiency coefficient in equation [16]. At the same time, it shows the interrelation of the engine torque increment with the increments of other engine state variables. Finally, by substituting equations [28] and [29] into equation [25], collecting and grouping coefficients for the same variables, the linearized and normalized equation of the engine shaft speed dynamics gains the following form:

$$\frac{d}{dt} \delta n_{sh} = a_{11} \delta n_{sh} + a_{13} \delta P_s + a_{14} \delta M_{exh} + a_{15} \delta T_{exh} + b_{11} \delta h_{fp} + k_{q_2} \delta u_p \qquad [30]$$

Likewise, the linearized and normalized version of the rest of the state variables in equation [22] can be obtained, resulting in the linearized state-space description of the engine propulsion system (uncontrolled part) in terms of variables finite increments in the following form:

$$\frac{d}{dt} \delta x = A\, \delta x + B\, \delta u, \quad \delta x = \left[\delta n_e, \delta n_{tc}, \delta P_s, \delta M_{exh}, \delta T_{exh} \right]^T, \quad \delta u = \left[\delta h_{fp}, \delta u_p \right]^T$$

$$\delta y = C\, \delta x$$

$$A = \begin{bmatrix} a_{11} & 0 & a_{13} & a_{14} & a_{15} \\ 0 & a_{22} & a_{23} & a_{24} & a_{25} \\ a_{31} & a_{32} & a_{33} & a_{34} & a_{35} \\ a_{41} & 0 & a_{43} & a_{44} & a_{45} \\ a_{51} & 0 & a_{53} & a_{54} & a_{55} \end{bmatrix}, \quad B = \begin{bmatrix} b_{11} & k_{q_2} \\ 0 & 0 \\ 0 & 0 \\ b_{41} & 0 \\ b_{51} & 0 \end{bmatrix}, \quad C = \begin{bmatrix} 1 & \cdots & 0 \\ \vdots & \ddots & \vdots \\ 0 & \cdots & 1 \end{bmatrix} \qquad [31]$$

The coefficients of the system matrix A and input matrix B are analytically bound up with the original nonlinear equation [22], and thus can easily be evaluated at arbitrary operating points of the propulsion system. Furthermore, the uncontrolled state-space representation of the propulsion system can be turned into a controlled version simply by expanding and combining the state matrix A and input matrix B with the linear part of the governor's state-space description [23]. The transformation results in the updated matrices and vectors:

$$\delta x = \left[\delta n_e, \delta n_{tc}, \delta P_s, \delta M_{exh}, \delta T_{exh}, \delta X_{efb}, \delta X_p \right]^T, \quad \delta u = \left[\delta u_p \right]^T$$

$$A = \begin{array}{l} \text{Engine} \\ \\ \\ \\ \\ \text{Governor} \end{array} \begin{bmatrix} a_{11} & 0 & a_{13} & a_{14} & a_{15} & 0 & \frac{b_{11}}{K_{su}} \\ 0 & a_{22} & a_{23} & a_{24} & a_{25} & 0 & 0 \\ a_{31} & a_{32} & a_{33} & a_{34} & a_{35} & 0 & 0 \\ a_{41} & 0 & a_{43} & a_{44} & a_{45} & 0 & \frac{b_{41}}{K_{su}} \\ a_{51} & 0 & a_{53} & a_{54} & a_{55} & 0 & \frac{b_{51}}{K_{su}} \\ b_{61} & 0 & 0 & 0 & 0 & a_{66} & a_{67} \\ b_{71} & 0 & 0 & 0 & 0 & a_{76} & a_{77} \end{bmatrix}, \quad B = \begin{bmatrix} k_{q_2} \\ 0 \\ 0 \\ 0 \\ 0 \\ 0 \\ 0 \end{bmatrix}, \quad C = \begin{bmatrix} 1 & \cdots & 0 \\ \vdots & \ddots & \vdots \\ 0 & \cdots & \frac{1}{K_{su}} \end{bmatrix} \qquad [32]$$

The obtained state-space description, either uncontrolled or controlled, defines the system's dynamic behavior in the time domain. However, in the context of propeller-engine interaction, the frequency domain behavior is of primary interest. Thus, the transition from the time domain to the frequency domain representation, in the form of the transfer function of the linear system from input, δu, to output, δy, can be easily obtained by applying the Laplace transformation to the state-space system in the following form:

$$W(s) = \frac{\delta y}{\delta u} = C(sI - A)^{-1} B, \quad s \equiv \frac{d}{dt} - \text{the Laplace operator}$$

[33]

$$H(\omega) = 20 \log_{10} |W(i\omega)|, [dB]$$

Equation [33] provides the plotting of Bode charts, which quantify the ratio of the system response magnitudes to the magnitude of the input disturbance in the range of frequencies. There are seven responses to the input disturbance of the inflow velocity in the context of the presented propulsion system.

Time and Frequency Domain Validation

The linearization comes with a cost: the model is only valid for small variations around the steady-state point. So, the important question is how the state-space linearized model compares to the numerical non-linear model in both the time and frequency domains. To get insights into how both models behave, a numerical simulation was implemented in MATLAB/Simulink. The Panamax-size bulk carrier is used as a prototype ship for the numerical model. The hull form was designed at the National Maritime Research Institute (NMRI) with a target speed of 14.5 kt at 90% MCR. The principal dimensions of the hull and propeller are listed in Table 1. The required engine power was assessed as a result of propeller-hull matching for the desired target speed. The engine particulars are listed in Table 2. It is assumed that a ship advances with a constant speed, U_0, in head waves and experiences longitudinal (surge) motion. As mentioned before, the axial component of the velocity field around the propeller influences the behavior of the propulsion engine directly, thus is the most important' for the investigation of wave-propeller-engine interaction (Bondarenko 2012, Taskar 2016).

The model of inflow velocity is composed of two terms (Nakamura 1975): due to the hull surge motion, u_{pm}, and due to the wave orbital motion, u_{pw}, as follows:

$$\begin{cases} u_p = u_{p_m} + u_{p_w} \\ u_{p_m} = (1 - w_p)\{U_0 - \omega_e \xi_a \sin(\omega_e t - \varepsilon_\xi)\} \\ u_{p_w} = \alpha_w \omega \zeta_w e^{-k z_p} \cos \chi \cos(\omega_e t - k x_p \cos \chi) \end{cases}$$

[34]

where ω_e is the encounter wave frequency, ξ_a and ε_ξ are the surge motion amplitude and phase, correspondingly; ω is the incident wave frequency, χ is the heading angle to waves, ζ_w is the wave amplitude, k is the wavenumber ($=2\pi/\lambda$) and λ is the wavelength, x_p and z_p are the coordinates of propeller position with respect to the hull centre of gravity, G. The dynamics of the subject hull dynamics as well as an effective wave amplitude coefficient α_w are discussed in details by Kitagawa (2019). The time histories of inflow velocity fluctuation in irregular waves are generated based on linear wave theory and detailed discussion is not in the scope of this paper.

Table 1: Principal particulars of a ship and propeller

Item	Design Value
L_{pp} (m)	217.0
B (m)	32.3
D (m)	12.2
Displacement (ton)	7.17e4
Service Speed U_0 (kt)	14.5
C_B	0.84
Propeller Series	Wageningen B
D_p (m)	6.6
Blades	4
Pitch Ratio	0.65

Table 2: Propulsion engine specification @ MCR

Engine Type	Mitsui-MAN S50ME-T9
No of Cylinders	6
Bore/Stroke, [mm/mm]	500/2214
Power, [kW]	9640
Speed, [rpm]	119
IMEP, [bar]	22
Scav. Air Pressure, [barA]	4.4

Figure 7, the engine envelope, visualizes the combined engine speed and power responses to the generated inflow velocity fluctuation in irregular waves, followed by figure 8, where the time histories of the corresponding engine state variables'

responses, relative to the MCR point, are shown. These graphs clearly show that the behavior of the state-space linear and non-linear models is indistinguishable, except for a slight difference in the exhaust gas temperature responses. This variation can be attributed to the nonlinearity of the characteristic. The presented results do not directly include the effect of resistance increase in waves, as mentioned from the beginning; equation [1] is neglected due to the negligible effect of varying added resistance in waves on the propulsion engine. Instead, the focus is put on understanding the responses in waves due to fluctuating inflow velocity, which indirectly includes the effect of the resistance fluctuation. Finally, figure 9 shows the responses in the frequency domain. A general observation is that both systems show similar response magnitudes for the range of frequencies typical for ocean waves. Additionally, as expected from the time-domain results, the magnitude of the exhaust temperature response is lower in the linear case.
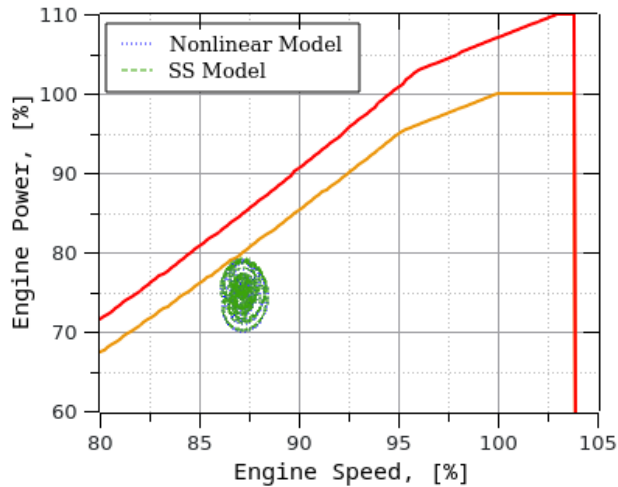

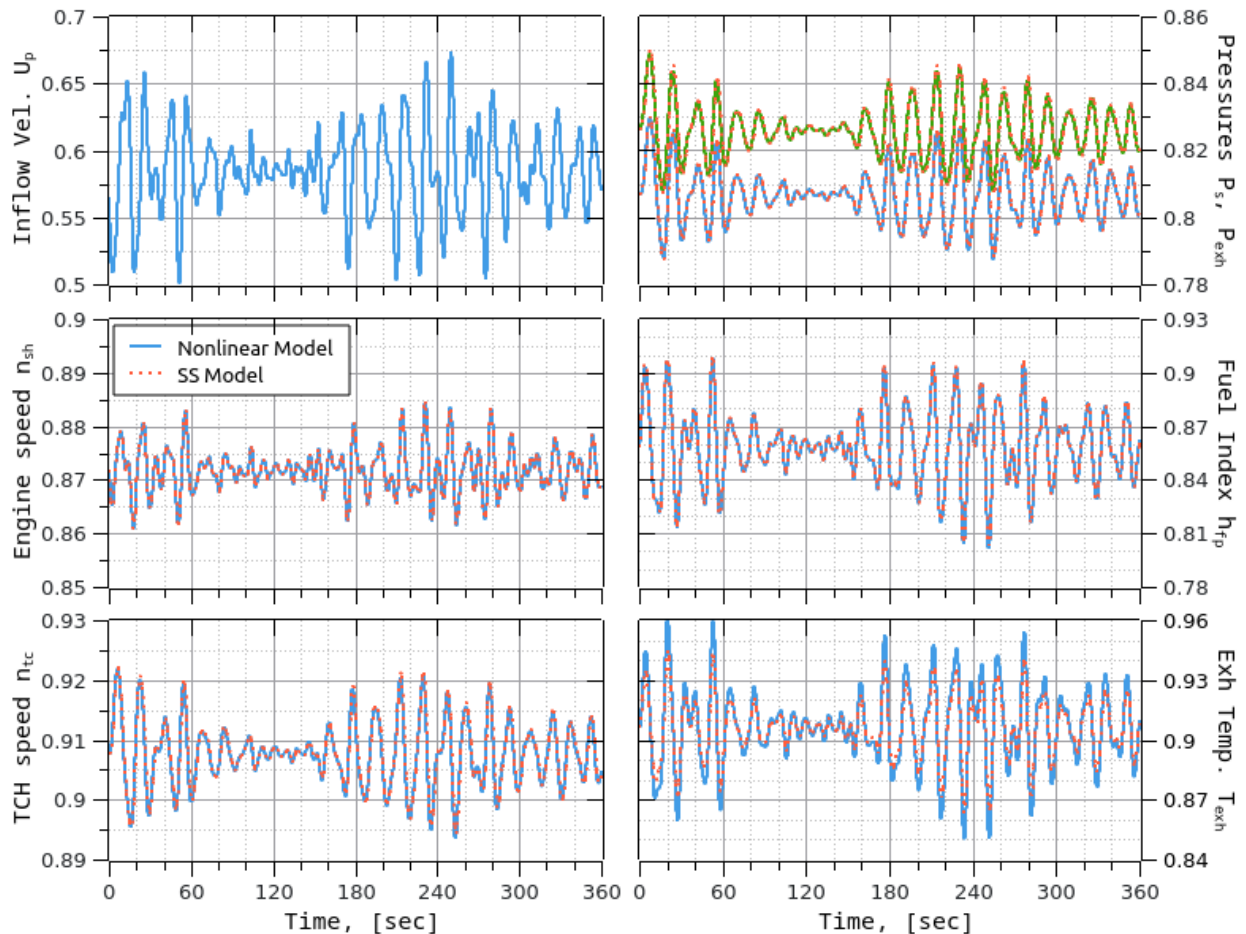Figure 7: Engine operating point response on the engine envelope

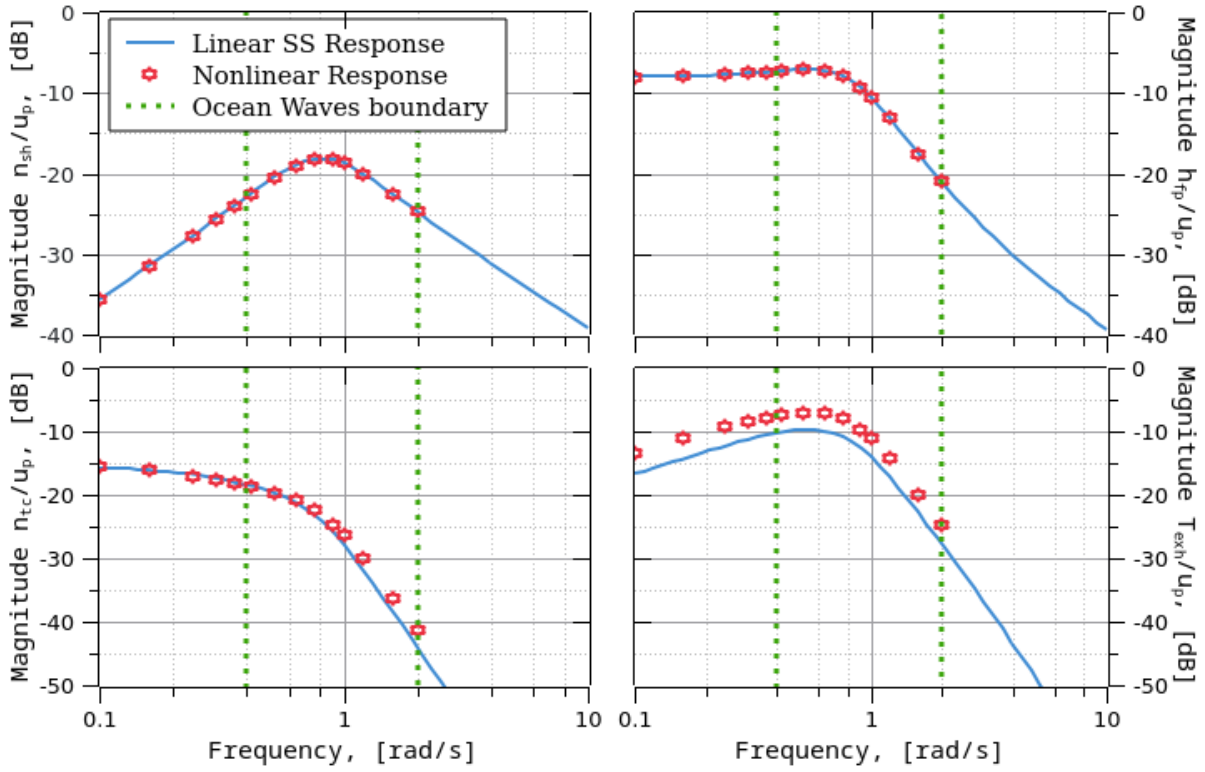Figure 8: Propulsion engine responses in time domain

Figure 9: Propulsion engine responses in frequency domain

Although the behavior of the linearized model compares fairly well with the full non-linear model, it has a major limitation: the non-linearity of the TLF that cannot be captured by a linear model in a straightforward manner. However, there is an approximate method of analysis in the frequency domain, also known as harmonic analysis, providing the replacement of each nonlinear element with a quasi-linear describing function. A brief description is provided in the subsequent subchapter.

Describing Function Representation of the TLF Function

One way to deal with a nonlinear system is to linearize it with the help of a finite increment method. Linearization in the time domain requires the system under consideration to be composed of continuous and differentiable characteristics. However, this approach is ill-suited for studying the limiting or detrimental effects of nonlinearity. On the other hand, harmonic linearization is a way of describing hard nonlinear functions in the frequency domain (Csaki 1972).

Let's assume the nonlinear transformation function $f(x,t)$ of the harmonic signal of the form $x(t) = a \sin(\omega t)$. The transformation results in the output $y(t) = f(a \sin(\omega t), t)$. The describing function gain, $N(a, \omega)$ is the fundamental harmonic of the Fourier series representation of this periodic output $y(t)$, divided by the input amplitude a, as follows:

$$y(t) \cong A_0(a,\omega) + N(a,\omega) \cdot a\, e^{j\omega t},$$

[35]

$$N(a,\omega) = q(a,\omega) + jq'(a,\omega)$$

The coefficients A_0, q, q' can be found through the Fourier series expansion of the non-linear transformation function $f(\bullet)$ as follows:

$$A_0 = \frac{1}{2\pi} \int\limits_0^{2\pi} f\left(a\sin\left(\Psi\right)\right) d\Psi, \quad \because \Psi \equiv \omega t$$

$$q = \frac{1}{a\pi} \int\limits_0^{2\pi} f\left(a\sin\left(\Psi\right)\right)\sin\left(\Psi\right) d\Psi \qquad\qquad [36]$$

$$q' = \frac{1}{a\pi} \int\limits_0^{2\pi} f\left(a\sin\left(\Psi\right)\right)\cos\left(\Psi\right) d\Psi$$

In the context of the nonlinear characteristic of TLF described by equation [24], and schematically shown in figure 10, the describing function gain can be derived as follows:

$$A_0\left(a\right) = \frac{1}{2\pi}\left[\int\limits_0^{\beta} a\sin\left(\Psi\right) d\Psi + \int\limits_{\beta}^{\pi-\beta} {}^+h_{fp}\, d\Psi + \int\limits_{\pi-\beta}^{2\pi} a\sin\left(\Psi\right) d\Psi\right]$$

$$= \frac{{}^+h_{fp}}{2} - \frac{{}^+h_{fp}}{\pi}\sin^{-1}\left(\frac{{}^+h_{fp}}{a}\right) - \frac{a}{\pi}\sqrt{1-\left(\frac{{}^+h_{fp}}{a}\right)^2}$$

$$q = \frac{1}{a\pi}\left[\int\limits_0^{\beta} a\sin^2\left(\Psi\right) d\Psi + \int\limits_{\beta}^{\pi-\beta} {}^+h_{fp}\sin\left(\Psi\right) d\Psi + \int\limits_{\pi-\beta}^{2\pi} a\sin^2\left(\Psi\right) d\Psi\right] \qquad [37]$$

$$= \frac{1}{2} + \frac{1}{\pi}\sin^{-1}\left(\frac{{}^+h_{fp}}{a}\right) + \frac{1}{\pi}\frac{{}^+h_{fp}}{a}\sqrt{1-\left(\frac{{}^+h_{fp}}{a}\right)^2}$$

$$q' = \frac{1}{a\pi}\left[\int\limits_0^{\beta} a\sin\left(\Psi\right)\cos\left(\Psi\right) d\Psi + \int\limits_{\beta}^{\pi-\beta} {}^+h_{fp}\cos\left(\Psi\right) d\Psi + \int\limits_{\pi-\beta}^{2\pi} a\sin\left(\Psi\right)\cos\left(\Psi\right) d\Psi\right]$$

$$= 0$$

$$\beta = \sin^{-1}\left(\frac{{}^+h_{fp}}{a}\right)$$

$$u(t) = y(t) = a\sin(\omega t), \qquad 0 \le \omega t \le \beta$$
$$u(t) = {}^+h_{fp}, \qquad\qquad \beta \le \omega t \le \pi - \beta$$
$$u(t) = y(t) = a\sin(\omega t), \quad \pi - \beta \le \omega t \le 2\pi$$
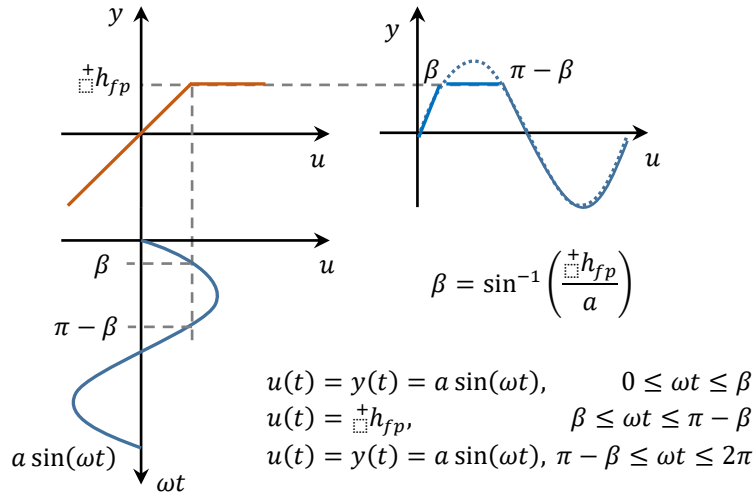
Figure 10: Schematic of nonlinear transformation of TLF

The components obtained in equation [37] define the describing function as frequency-invariant and input amplitude-dependent, though. In order to confirm the obtained characteristics, a simple numerical experiment was set up: a harmonic signal of varying amplitude at a single frequency passes through the saturation non-linearity, and the estimated amplitudes ratio is plotted in figure 11 along with the corresponding describing function. The presented results of the numerical simulation suggest the non-linearity analysis capability by the describing function method.

Finally, it should be observed that the saturation type non-linearity, such as TLF, also introduces the DC component (A_0), and to some extent, the AC component ($N(a)$) is dominant; however, the larger the amplitude, the larger the bias. Definitely, in

harsh sea conditions when the engine operation in close vicinity of the limit is inevitable, the effect of the DC component becomes prominent, exacerbating the safety concerns of propulsion system operation. For the purpose of this research, investigating the wave-propeller-engine interaction, only the AC component is considered at the moment, while the simultaneous consideration of both components will be left for future analysis.
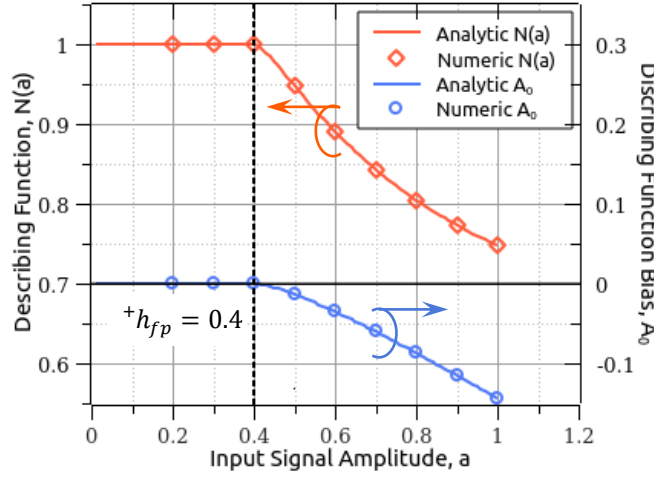

Figure 11: Describing function for saturation non-linearity

State-Space Model of the Propulsion System with TLF in Frequency Domain

The describing function method has traditionally been used for two primary purposes: limit-cycle stability analysis and characterizing the input-output behavior of a non-linear system in the frequency domain. In this paper, the focus is put on the latter purpose, particularly to determine the amplitude-dependent frequency response of a nonlinear system.

The TLF is placed between the governor and the engine to saturate the fuel pump index input to the engine and prevent thermal overload. Thus, the describing function coefficient, $N(a)$, is introduced to the system matrix A, to the part related to the governor-engine interface, as shown by equation [38], and delivers the quasi-linear response function as in equation [39]

$$\delta x = \left[\delta n_e, \delta n_{tc}, \delta P_s, \delta M_{exh}, \delta T_{exh}, \delta X_{efb}, \delta X_p\right]^T, \quad \delta u = \left[\delta u_p\right]^T$$

$$
\begin{array}{c}
\text{Engine} \\
\\
A = \\
\\
\text{Governor}
\end{array}
\left[
\begin{array}{ccccccc}
a_{11} & 0 & a_{13} & a_{14} & a_{15} & 0 & \frac{b_{11}}{K_{su}}N(a) \\
0 & a_{22} & a_{23} & a_{24} & a_{25} & 0 & 0 \\
a_{31} & a_{32} & a_{33} & a_{34} & a_{35} & 0 & 0 \\
a_{41} & 0 & a_{43} & a_{44} & a_{45} & 0 & \frac{b_{41}}{K_{su}}N(a) \\
a_{51} & 0 & a_{53} & a_{54} & a_{55} & 0 & \frac{b_{51}}{K_{su}}N(a) \\
b_{61} & 0 & 0 & 0 & 0 & a_{66} & a_{67} \\
b_{71} & 0 & 0 & 0 & 0 & a_{76} & a_{77}
\end{array}
\right],
\quad B = \left[
\begin{array}{c}
k_{q_2} \\
0 \\
0 \\
0 \\
0 \\
0 \\
0
\end{array}
\right],
\quad C = \left[
\begin{array}{ccc}
1 & \cdots & 0 \\
\vdots & \ddots & \vdots \\
0 & \cdots & \frac{1}{K_{su}}
\end{array}
\right]
\qquad [38]
$$

$$W(i\omega, a) = \frac{\delta y}{\delta u} = C\left[i\omega I - A(a)\right]^{-1} B \qquad [39]$$

Here, a stands for the amplitude of the governor's response before the TLF, that is:

$$a \equiv \delta h_{fp} = \left|W(i\omega, a)\right|\delta u_p, \quad C = \left[
\begin{array}{ccc}
0 & \cdots & 0 \\
\vdots & \ddots & \vdots \\
0 & \cdots & \frac{1}{K_{su}}
\end{array}
\right] \qquad [40]$$

Thus, to produce the frequency response of such a quasi-linear amplitude-dependent response function, an iterative solution is required until the convergence of the describing function value. The elaborated procedure is as follows: set a specific value for δu_p from a range of input amplitudes covering the expected operating range of the system and set a range of frequencies $[\omega_{min}, \omega_{max}]$ to span a frequency range of interest. Then, set $N(a) = 1$ and evaluate the amplitude of response, a, for every frequency in the range, update $N(a)$ and repeat the calculation until the convergence. It was found that a converged solution appears within a few iteration steps.

To illustrate the frequency response of the state-space system given the TLF activation, the simulation condition is set similar to that of figure 7, where the operating point is close enough to the limit line. To generate the amplitude-dependent DF, the six inflow velocity amplitudes in the range [0.08…0.20] were selected, and a set of frequencies covering the typical range of the ocean waves. Figure 12 illustrates the evolution of the describing function magnitude in the frequency domain. It is evident that the larger the input disturbance, the larger the response of the governor and, thus, the activation of the TLF function. Furthermore, figure 13 shows the frequency response of the propeller-engine system, and, as evident, the engine speed response increases as the input disturbance increases. This is because the increasing response, X_{pp}, of the governor linear part, also shown in figure 13, cannot reach the engine because of the TLF, whereas the response of the fuel pump index, h_{fp}, is suppressed. As for the air supply subsystem, including the compressor, receivers, and turbine, whose response is indicated by the TC rotating speed, n_{tc}, the effect of TLF is negligible owing to the large inertia.

Although the demonstrated effect of TLF is relatively small, it can be prominent for other operating points and dynamic properties of the speed control system, and the developed approach allows for the evaluation of various conditions in a straightforward and integrated manner.
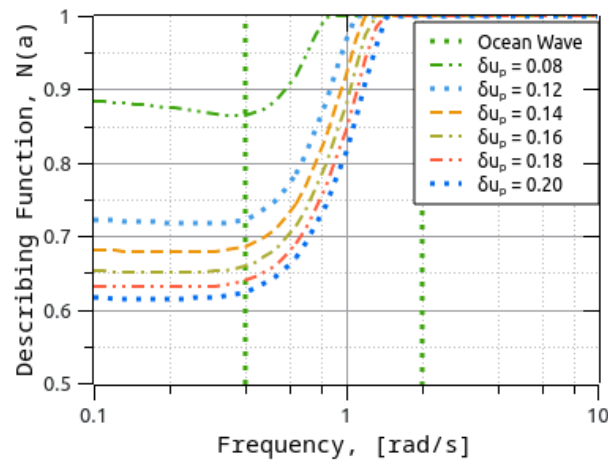

Figure 12: Describing function coefficient in frequency domain for a range of amplitudes
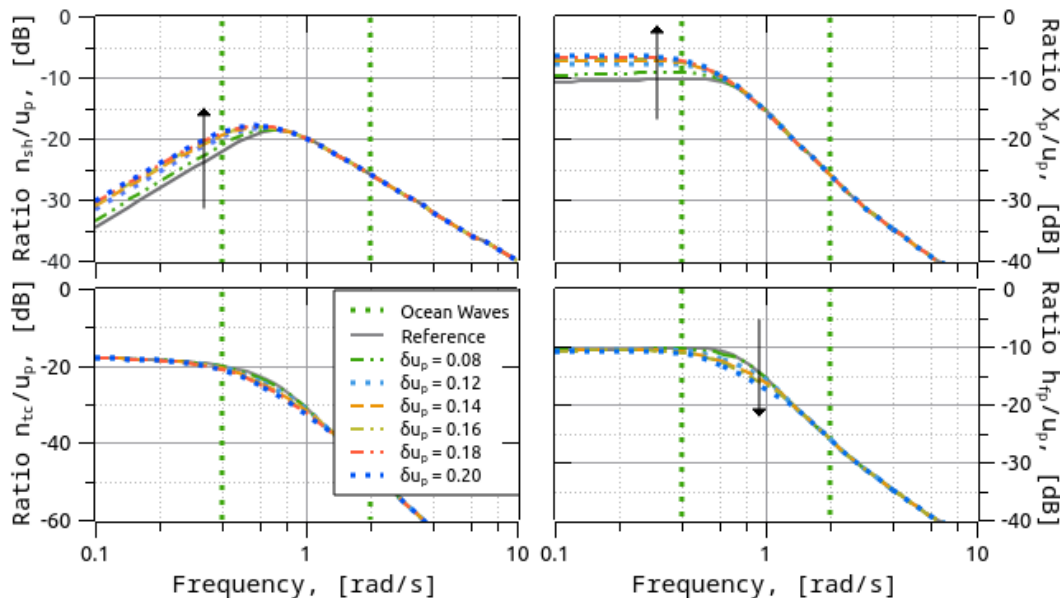

Figure 13: Frequency response of propeller-engine system in view of the TLF activation

CONCLUSIONS

Frequency-response techniques and the use of response functions are valuable tools in the analysis of the ship propulsion system behavior in waves. However, accurate calculation of the propulsion system response function requires detailed information about characteristics intrinsic to constituent components. This paper proposes the digital-twin-enabled response function analysis technique for the problem of wave-propeller-engine interaction assessment. The core part of the digital twin is the nonlinear, fully parametrized model of propeller-engine dynamics. The parameters identification framework from past research ensures that models are tailored to the specific ship in-service. The companion linearized state-space model was derived analytically based on the structure of the digital twin. A remarkable aspect of the developed linearized state-space model is the introduction of the air supply subsystem (compressor, receivers, and turbine), which has a notable effect on engine performance. The coefficients of the derived state-space system are bound up with the nonlinear models underlying the digital twin. Thus, at any point in the ship operation, reflected by the digital twin, the state-space system matrices can be readily obtained, and then a variety of analyses can be performed. This is valid only under moderate sea conditions, though. On the other hand, in adverse sea conditions, the increased propeller load forces the engine operating point to move closer to the upper bound of the engine operation limit. At the same time, significant propeller torque fluctuations occur. As a rule, the governors of modern engines are equipped with torque-limiting functions, preventing the engine from overloading, and simultaneously restricting the maneuverability of the ship. The latter circumstance has raised serious safety concern about ships with reduced propulsion power, used for better energy efficiency (Shigunov 2018). The presence and activation of torque saturation make the problem of propeller-engine interaction highly nonlinear. Therefore, it is desirable to extend the analysis of linearized state-space systems to the consideration of systems with nonlinear components such as TLF. In this work, the effect of the nonlinear function was approximated by using the theory of harmonic linearization. Specifically, the output of the nonlinear function is represented by its Fourier series by assuming a pure sinusoidal signal of constant amplitude with no bias at the input and no subharmonics at the output. Thus, the describing function is then defined as the complex ratio of the fundamental term of the output to the input sinusoid. A simple example considered in the paper showed that the system responses to a variety of disturbance amplitudes can be studied in the frequency domain utilizing the linear system theory.

To wrap up, this paper proposes a synthetic approach to evaluating and assessing a ship's propulsion system. A digital twin precisely reflects the characteristics intrinsic to the ship in-service, and the companion state-space system, bound up with the digital twin, provides a foundation for wave-propeller-engine interaction analysis in the frequency domain. The harmonic linearization extends the technique to consider the nonlinearity of TLF. All components are mutually supportive, ensuring that the data feedback from the ship in service can be used to assess propulsive performance in waves and review future ship designs.

Besides all the aforementioned aspects, there is also a desire to extend the technique by combining the wave-hull interaction problem, providing a holistic assessment of ship operation in actual sea conditions, as shown by Bondarenko (2012). The required component is the response function of hull motions in waves, and Nielsen (2021, 2022) proposed a simple and practical method that can be used to tune the transfer function from in-service data of hull response measurement. This is the subject of ongoing research.

CONTRIBUTION STATEMENT

Author 1: Conceptualization; propeller-engine interaction methodology; describing function analysis; writing – original draft. **Author 2:** Wave-hull interaction methodology; review and editing.

REFERENCES

Bondarenko, O., Kashiwagi, M. (2011), Statistical Consideration of Propeller Load Fluctuation at Racing Condition in Irregular Waves. *J. of Mar. Sci. and Techn.*, 16(4), 402-410

Bondarenko, O, Kashiwagi, M. (2012). Ensuring safe operation of ship propulsion plant in extreme sea condition. *In Proc.: 11th International Marine Design Conference*, 3, 83-96

Bondarenko, O., Fukuda, T. (2018). Intelligent Air Management for Ultimate Flexibility of Ship Propulsion Plant Operation. Part 1: Experiment and Simulation. *J. Japan Institute of Marine Engineers*, 53

Bondarenko, O., Fukuda, T., Kitagawa Y., Omiya T. (2020). Problem of Identification and Adaptation of Main Engine Digital Twin Based on Operational Data. *J. Japan Institute of Marine Engineers*, 57(2), 30-34

Bondarenko, O., Kitagawa, Y., et.al. (2023). Development of a free-Running model test methodology for evaluation of a full-scale ship propulsion system performance. CIMAC Congress, Paper No.328

Bondarenko, O., Fukuda, T., Miura, S. (2023). Empowering Propulsion Engine Digitalization Utilizing Digital Twin, Kalman Filter and Data Assimilation. *Jpn Soc. Nav. Arch. Ocean Eng.*, 36, 95-101

Csaki, F. (1972). *Modern Control Theories: Nonlinear, Optimal and Adaptive Systems*, Budapest: Akademiai Kiado

Sui, C., et.al. (2022). Effects of Adverse Sea Conditions on Propulsion and Maneuvering Performance of Low-Powered Ocean-Going Cargo Ship. Ocean Engineering, 254

Gorb, S.I. (1989). *Analysis of automatic speed control systems of ship's diesel engine plants*. Moscow: Mortechinformreklama (In Russian)

Hendrics, E. (1989). Mean value modelling of large turbocharged two-stroke diesel engines. *SAE*, technical paper No 890564

Kim, SK, Naito, S., Nakamura, S. (1985). Propulsive performance of lower speed ship in a seaway. *J Kansai Soc Naval Arch Japan*, 196

Kitagawa, Y., Bondarenko, O., et al. (2019). An experimental method to identify a component of wave orbital motion in propeller effective inflow velocity and its effects on load fluctuations of a ship main engines in waves. *App Ocean Res.*, 92

Mezherickiy, A.D., (1971). *Turbochargers of the Diesel engines*. Leningrad: Shipbuilding (in Russian)

Medica V., (1988). Simulation of turbocharged diesel engine driving electrical generator under dynamic working conditions. Manuscript of dissertation: University of Rijeka. Croatia

Nakamura, S., Hosoda, R., Naito S. (1975). Propulsive performance of a container ship in waves (3rd report). *J.Kansai Soc Nav Archit Japan.*, 158, 37–46 (in Japanese).

Naito, S, Nakamura, S, and Hara, S. (1979). On the prediction of speed loss of a ship in waves. *J Kansai Soc Naval Arch Japan,* 146

Nielsen, U.D., Mounet, R.E.G., Brodtkorb, A.H. (2021). Tuning of transfer functions for analysis of wave-ship interactions. *Mar. Struct.*, 79, 103029

Nielsen, U.D., Mounet, R.E.G., Brodtkorb, A.H. (2022). Parametrized transfer functions with associated confidence bands. *App Ocean Res.*, 125, 103250

Shigunov, V. (2018) Manoeuvrability in adverse conditions: rational criteria and standards. *J. Mar. Sci and Tech.*, 23(4), 958-976

Stapersma, D., Vrijdag, A. (2017). Linearization of a ship propulsion system model. *J. Ocean Eng.*, 142, 441-457

Taskar, B., Yum, K., K., et.al. (2016). The effects of waves on engine-propeller dynamics and propulsion performance of ships. *Ocean Eng.*, 122, 262–277

Theotokatos, G. (2010). On the cycle mean value modelling of a large two-stroke marine diesel engine. *Proc. IMechE Part M: J. Engineering for the Maritime Environment*, 224, 193-205.

Vrijdag, A., Stapersma, D. (2017). Extension and application of a linearized ship propulsion system model. *J. Ocean Eng*. 143, 50-65

Xiros, N. (2002). *Robust control of diesel ship propulsion*. Springer